RSC Advances

PAPER

View Article Online
View Journal | View Issue

Cite this: *RSC Adv.*, 2019, **9**, 15642

Synthesis of bimetallic–organic framework Cu/Co-BTC and the improved performance of thiophene adsorption†

Fuping Tian,* Chenxia Qiao, Renyu Zheng, Qiaofeng Ru, Xin Sun, Yifu Zhang and Changgong Meng

Received 30th March 2019
Accepted 13th May 2019

DOI: 10.1039/c9ra02372k

rsc.li/rsc-advances

A bimetallic–organic porous material (Cu/Co-BTC) with a paddle-wheel structure has been successfully synthesized by a solvothermal approach. The as-synthesized materials were characterized by XRD, SEM, ICP-AES, UV-Vis, TGA and N_2 adsorption at 77 K. The prepared Cu/Co-BTC samples were investigated in thiophene (TP) adsorption from model gasolines by the fixed bed adsorption method at 298 K. The results showed that only a small amount of Co could be successfully introduced into the framework of HKUST-1, and the introduction of Co had little effect on the crystalline structure, morphology, porosity, and thermal stability. The bimetallic Cu/Co-BTC with a Cu/Co ratio of 174 displayed significantly improved adsorption desulfurization performance, showing an increase in breakthrough volume by 30% compared with HKUST-1, implying that the central metal in the MOF plays an important role in adsorption desulfurization. The addition of toluene or cyclohexene (3.20–3.30 vol%) as a competitor in the model gasoline led to a decline in desulfurization performance, especially when cyclohexene was added. The bimetallic Cu/Co-BTC showed a slight loss in breakthrough volume by only 5% after regenerating 7 times, displaying an excellent regeneration property.

1 Introduction

Deep desulfurization for ultra-clean fuels has attracted more and more attention worldwide due to more stringent environmental regulations and increasing demand for ultra-clean fuels.[1–4] Several methods including physical, chemical and biological techniques have been investigated for removing sulfur-containing compounds (SCC) from oils. Specifically speaking, they are hydrodesulfurization (HDS),[5,6] biodesulfurization (BDS),[7,8] oxidative desulfurization (ODS),[9,10] extractive desulfurization (EDS)[11,12] and adsorption desulfurization (ADS).[13–33] Considering some advantages of ADS, such as mild operation conditions, low operating cost, no need for hydrogen, and showing little effect on the properties of oils,[2–4] ADS is regarded as one of the most promising techniques to reduce sulfur concentration to ultralow levels (less than 5 ppm S).

So far, a bunch of adsorbents have been reported for desulfurization, such as metal oxides,[13] active carbon,[14] zeolites,[15–17] mesoporous materials[18,19] and metal–organic framework (MOF) materials.[20–34] Among them, MOFs are getting more and more interest in adsorption desulfurization in recent years because of the high specific surface areas, highly ordered three-dimensional pore structures, and easy modification of pore size and shape.[20] Based on these advantages, some pristine MOFs have been investigated in adsorption desulfurization. In 2008, Matzger and co-workers[20] published the first report in removing benzothiophene (BT), dibenzothiophene (DBT) and dimethyldibenzothiophene (DMDBT) using HKUST-1, UMCM-150, MOF-5, MOF-505, and MOF-177 as adsorbents, and they found that the adsorption capacity is determined by pore size and shape, as well as the interaction between the SCC and the framework. In recent years, some researchers made some efforts to improve the desulfurization performance by modifying the virgin MOFs material through introducing Cu^+ into pristine MOFs,[21–23] or supporting/encapsulating ionic liquid on MIL-101 (Cr).[24,25] Besides these, some MOFs built by the same ligand but different metal ions have also been studied to investigate the effect of central metals on the desulfurization performance, since the coordinated unsaturated central metals are considered as the adsorption sites for desulfurization.[26–33] Khan *et al.*[26] studied the removal of BT using three analogous MOFs MIL-53(Al, Cr, V) and found that MIL-47(V) showed the best adsorption capacity. This result was ascribed to the highest acidity of MIL-47(V), though the origin of acidity was not clear. Considering the results in the literatures that central metals play important role in adsorption desulfurization, a new strategy to improve the desulfurization performance by doping

School of Chemistry, State Key Laboratory of Fine Chemicals, Dalian University of Technology, 2 Linggong Road, P. O. Box 288, Dalian 116024, China. E-mail: fptian@dlut.edu.cn; Fax: +86-411-84706313; Tel: +86-411-84708901

† Electronic supplementary information (ESI) available. See DOI: 10.1039/c9ra02372k

other metals into the framework was proposed recently.[27–29] Dai and co-workers reported the synthesis of bimetallic Ni/Cu-BTC,[27] Zn/Cu-BTC,[28] V/Cu-BTC[29] and trimetallic Ni/Zn/Cu-BTC[30] by solvothermal approach, which displayed the same crystalline structure as the monometallic counterpart HKUST-1. And they found that the trimetallic MOFs exhibited a higher desulfurization capacity than bimetallic ones and HKUST-1, due to the synergistic effect of different kinds of metals. Our previous work[31,32] investigated thiophene (TP) adsorption in the presence of toluene and cyclohexene over HKUST-1 and Ni-BTC, the two isostructure adsorbents built by the same ligand but different metals displayed different adsorption selectivities to TP, and the different adsorption models of three adsorbates inferred by the adsorption isotherms demonstrated again that the central metal in MOF does play crucial role in ADS. In this manuscript, we focused on the synthesis of bimetallic Cu/Co-BTC in which Cu^{2+} cations were partly substituted by Co^{2+}. The choice of Co is based on the consideration that Cu^{2+} and Co^{2+} have similar ionic radius (Cu^{2+}: 72 pm, Co^{2+}: 74 pm) and both can act as coordination unsaturated central metal sites in MOFs with identical crystalline structure. The effect of the second metal cobalt on the properties of the resultant MOF was studied and the breakthrough curves of Cu/Co-BTC and HKUST-1 were investigated and compared at room temperature and atmospheric pressure.

2 Experimental

2.1 Materials and model gasolines

Analytical grade reagents, such as cobalt nitrate ($Co(NO_3)_2 \cdot 6H_2O$, >98.5%), copper nitrate ($Cu(NO_3)_2 \cdot 3H_2O$, >99.5%), ethanol (>99.7%), toluene (>99.5%), cyclohexene (>98%) cyclohexane (>99.7%), and *N*,*N*-dimethylformamide (DMF, >99.5%) were purchased from Tianjin Damao Chemical Co. Ltd. 1,3,5-Benzenetricarboxylic acid (H_3BTC, >98%) was purchased from Aladdin Chemistry Co. Ltd, and thiophene (99%) was purchased from J&K Chemical Co. Ltd. All chemicals were used as purchased without further purification.

TP as a model organic sulfur compound was dissolved in cyclohexane to make model gasoline (MG). Toluene and cyclohexene were selected as aromatic and olefin competitors, respectively. The sulfur contents of different MGs were *ca.* 100 mg S L^{-1}. Detailed compositions of the MGs are listed in Table 1.

2.2 Synthesis of Cu/Co-BTC

Cu/Co-BTC-*x* (*x* stands for Cu/Co molar ratio in the MOF product) was synthesized according to the following procedure. $Cu(NO_3)_2 \cdot 3H_2O$, $Co(NO_3)_2 \cdot 6H_2O$, and H_3BTC (1.00 g, 4.8 mmol) were added together in 51 mL of solution consisting of equal volume of DMF, deionized water, and ethanol. The obtained mixture treated by ultrasonication for 30 min was then transferred into vials. The vials were sealed and placed in an oven, heated to 358 K at a ramping rate of 0.5 K min^{-1} and maintained for 20 h. The product was separated by filtration, washed with absolute ethanol for several times. For comparison, the MOF material in the absence of metal Co, *i.e.* HKUST-1, was synthesized according to the procedure reported in our previous work.[31]

2.3 Characterization

The X-ray diffraction (XRD) pattern of the synthesized Cu/Co-BTC was collected in 2θ range of 5–50° using a X'pert diffractometer with Cu K_α radiation ($\lambda = 1.5418$ Å), operated at 40 kV and 40 mA. The thermal stability of Cu/Co-BTC was detected using a thermogravimetric analysis (TGA) unit (STA-499C). About 10 mg of the sample was heated in the flow of nitrogen (60 mL min^{-1}) with a ramp of 10 K min^{-1} from 298 K to 873 K. N_2 adsorption–desorption isotherm of Cu/Co-BTC was measured on an Quantachrome apparatus at 77 K. Prior to the measurement, the sample was dried at 423 K overnight in a vacuum oven. Then about 100 mg of the sample was degassed at 473 K for 4 h. The total surface area was determined by Langmuir method. The micropore volume and the micropore surface area were obtained by *t*-plot method. The scanning electron microscopy (SEM) imaging of the sample was performed on a Quanta 450 instrument operated with an acceleration voltage of 20 kV. Prior to the observation, the sample was sputter-coated with a gold layer to increase its conductivity. The Cu/Co molar ratios in the products were measured by ICP-AES (inductively coupled plasma-atomic emission spectrometry) on a PerkinElmer Nex ION 300D instrument. The UV-Vis diffuse reflectivity spectra were collected by UV-550 of JASCA company from 200 to 800 nm.

2.4 Adsorption desulfurization and regeneration

Adsorption desulfurization performance of Cu/Co-BTC samples was evaluated in a fixed-bed flow reactor with an inner diameter of 6 mm and a length of 300 mm. About 0.50 g of pre-dried adsorbent was firstly heated at 493 K for 2 h under N_2 (40 mL min^{-1}) in order to remove the solvents and physically adsorbed water and then cooled to room temperature in N_2. At 303 K and atmospheric pressure, MG1 ($c_0 = 101.2$ mg S L^{-1}) was pumped into the fixed-bed flow reactor in a quartz column at a flow rate of 0.25 mL min^{-1}. Sulfur content of the effluent was

Table 1 The compositions of model gasolines

Model gasoline	Sulfur content (mg S L^{-1})	Compositions	n_{CHE}/n_{TP}	CHE[a] (vol%)	n_{Tolu}/n_{TP}	Tolu[b] (vol%)
MG1	101.2	TP/cyclohexane				
MG2	105.2	TP + CHE/cyclohexane	100	3.20		
MG3	101.4	TP + tolu/cyclohexane			100	3.30

[a] CHE = Cyclohexene. [b] Tolu = Toluene.

sampled at an interval of 10 min and analyzed by micro-coulometry. When the sulfur content of the effluent achieved 0.05 c_0, the effluent volume at this point was considered to be the breakthrough volume, which was taken to calculate the breakthrough sulfur capacity (mmol S g^{-1}).

$$q = \frac{c_0 V}{m} \times 10^{-3}$$

where V is the breakthrough volume (mL) of the effluent, and m is the mass of the adsorbent (g).

The regeneration was carried out as follows: the used Cu/Co-BTC was swept by N_2 firstly at room temperature for 1 h and then at 423 K for 2 h. After that, it was cooled to room temperature in N_2. At 303 K and atmospheric pressure, the breakthrough experiment of the regenerated Cu/Co-BTC was run as the above procedure. The regeneration was performed for seven times to investigate the reusability of Cu/Co-BTC.

3 Results and discussion

3.1 Properties of the adsorbents

The molar ratio of Cu to Co in the final product can be adjusted by modulating the relative amount of precursors $Cu(NO_3)_2 \cdot 3H_2O$ and $Co(NO_3)_2 \cdot 6H_2O$ with the maintenance of $n_{(Cu+Co)} : n_{BTC} = 1.75$. All products were in the form of homogeneous blue powder, except for that synthesized by a precursor with $n_{Cu} : n_{Co} = 10 : 90$. It can be clearly seen from the photograph (Fig. S1†) that some blue powder and dark purple needle species coexist in the small vial. The products in different forms were carefully separated and collected for XRD measurement. The patterns in Fig. S2† confirm that the two species are entirely different from each other in crystallinity, implying that too much $Co(NO_3)_2 \cdot 6H_2O$ in precursors led to a failure in the synthesis of Cu/Co-BTC sample. The precursors with $n_{Cu} : n_{Co}$ ratio ranging from 20 : 80 to 90 : 10, however, can bring about successful synthesis of bimetallic MOF materials. The XRD patterns shown in Fig. 1 illustrated that the homogeneous blue powders displayed the same peaks as HKUST-1, indicating a crystalline structure consisting of paddle-wheel units in analogy to HKUST-1 without any impurity.[35]

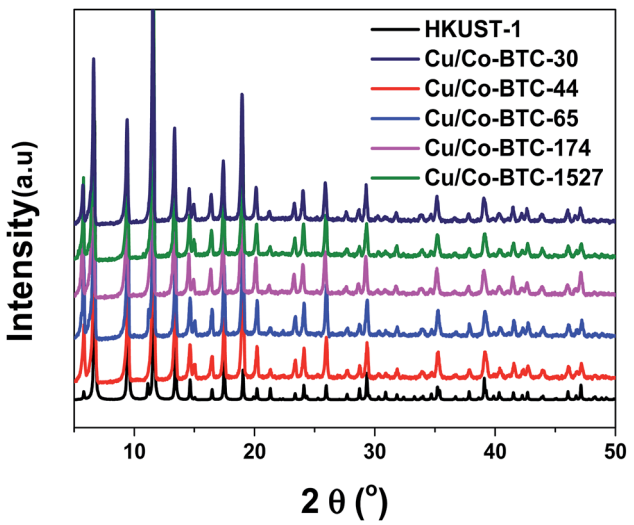

Fig. 1 XRD patterns of Cu/Co-BTC samples with different Cu/Co ratios.

The Cu/Co ratios in the pure phase Cu/Co-BTC samples measured by ICP-AES were listed in Table S1.† As can be seen, the dominant amount of Co salt in the precursor solutions (entry 2–4) didn't led to a higher Co content in the final Cu/Co-BTC samples, for instance, $n_{Cu} : n_{Co}$ in the resultant MOF was detected to be 30, even though $n_{Cu} : n_{Co}$ in the precursor solution was controlled at 20 : 80. This result indicated that Co^{2+} ions, compared with Cu^{2+} ions, are much more difficult to interact with the ligand molecules and construct the framework. A monotonous drop in Co content in the resultant Cu/Co-BTC samples was observed when decreasing the Co content in the precursor mixture. The above results displayed that changing the Cu/Co ratios in the precursor mixtures in a wide range can only adjust the Co contents in the resultant Cu/Co-BTC samples in a small range at a very low level, which is quite different from the results reported in Zn/Cu-BTC and Ni/Cu-BTC cases, where the ratios of the two metals in bimetallic MOFs are almost the same as those in the precursor mixtures.[27,28]

The textural properties of Cu/Co-BTC-65 and Cu/Co-BTC-174 were tabulated in Table 2. It can be seen that the Langmuir specific surface areas (1237 and 1214 $m^2\ g^{-1}$) and the pore volumes (0.44 and 0.43 $cm^3\ g^{-1}$) of the two samples were almost the same, and they are both slightly less than those of HKUST-1, suggesting that the low Co content in the framework had little effect on the porosity of Cu/Co-BTC samples. Moreover, the mesopore volume of 0.02 $cm^3\ g^{-1}$ manifested a microporous characteristic for both samples.

The SEM images of HKUST-1 and Cu/Co-BTC-174 shown in Fig. 2 displayed regular octahedral morphology, with edge length of about 15 μm, suggesting that Co-doping didn't bring about any change in the morphology of HKUST-1.

Thermal stability is one of the important factors that determines whether an adsorbent is suitable for desulfurization research. The TG and DTA curves of Cu/Co-BTC-174 were displayed in Fig. 3, and those of HKUST-1 were also included for comparison. It can be seen that three steps of mass loss can be observed for Cu/Co-BTC-174, which is very similar to HKUST-1. The evident mass loss about 25% between 300–370 K was ascribed to the removal of physically adsorbed water and a part of solvent in the pores. A continuous mass loss between 380–600 K corresponded to the removal of DMF, its higher removal temperature than other solvents is attributed to its higher boiling point (425.95 K) and the strong interaction between DMF molecule and the framework.[36] A significant mass loss at 600–650 K was assigned to the decomposition of the organic ligand in the framework, which was confirmed by the XRD pattern of the residue (not shown for brevity). The similar TG curves of Cu/Co-BTC-174 and HKUST-1 indicate that the introduction of a small amount of Co in the framework had little effect on the thermal stability of HKUST-1.

Table 2 The textural properties for different samples

Sample	$S_{Langmuir}$ [a] ($m^2\ g^{-1}$)	S_{micro} [b] ($m^2\ g^{-1}$)	S_{meso} ($m^2\ g^{-1}$)	V_{Total} ($cm^3\ g^{-1}$)	V_{micro} ($cm^3\ g^{-1}$)	V_{meso} ($cm^3\ g^{-1}$)
Cu/Co-BTC-65	1237	892	345	0.44	0.42	0.02
Cu/Co-BTC-174	1214	882	332	0.43	0.41	0.02
HKUST-1[c]	1347	1211	136	0.51	0.47	0.04

[a] Langmuir method. [b] *t*-Plot method. [c] Data from ref. 30.

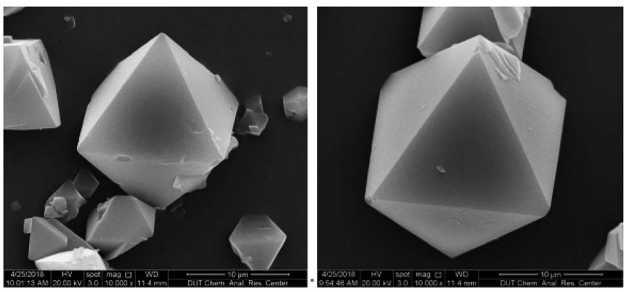

Fig. 2 SEM images of HKUST-1 (left) and Cu/Co-BTC-174 (right).

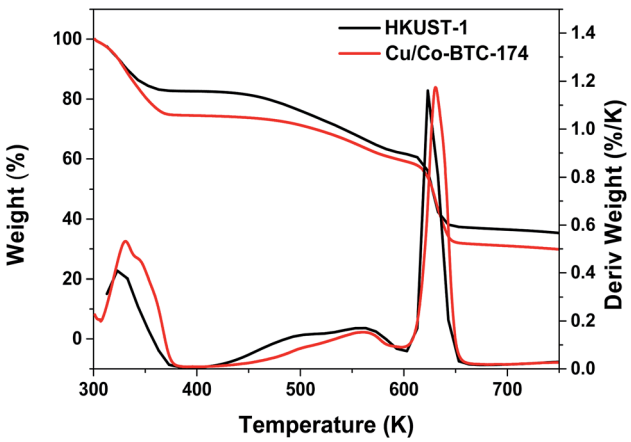

Fig. 3 TG and DTG curves of HKUST-1 and Cu/Co-BTC-174.

The Co^{2+} species introduced into HKUST-1 may exist as either oxides or central metal, UV-Vis test was conducted to investigate the state of Co species in Cu/Co-BTC samples. The results were displayed in Fig. 4. As can be seen, two absorption peaks at 310 nm and 230 nm were observed for HKUST-1 in the ultraviolet region, which belong to the π–π* transition in the ligand molecule.[37] It is worth noting that the absorption peak at 310 nm for HKUST-1 shifted blue to 304 nm for Cu/Co-BTC, which was due to an increase in the electronic transition energy level in the ligand arising from the coordination of organic ligands with different central metals.[38] The blue shift, therefore, indicated that Co species in Cu/Co-BTC sample replace part of the central metal Cu and act as the metal knots in the framework. Moreover, the absence of CoO_x in XRD patterns of Cu/Co-BTC samples (shown in Fig. 1) confirmed that Co species existed in the form of central metal rather than oxides.

3.2 Desulfurization performance of Cu/Co-BTC samples

The breakthrough curves of TP adsorption over HKUST-1 and Cu/Co-BTC samples were shown in Fig. 5. It can be seen that HKUST-1 displayed a breakthrough volume of 93 mL g^{-1}, exhibiting an excellent desulfurization performance. When different amount of Co was introduced into the framework, the resultant bimetallic Cu/Co-BTC samples showed evidently improved breakthrough volumes to different extent. The breakthrough volumes increased in the following order: Cu/Co-BTC-221 (106 mL g^{-1}) < Cu/Co-BTC-44 ≈ Cu/Co-BTC-65 (110 mL g^{-1}) < Cu/Co-BTC-174 (121 mL g^{-1}), indicating that the desulfurization performance of Cu/Co-BTC didn't increase monotonously as the Co content increased. The best desulfurization performance of 121 mL g^{-1} was observed on Cu/Co-BTC-174, showing an enhancement in breakthrough volume by 30%. The sulfur capacity of Cu/Co-BTC-174 at the breakthrough point was calculated to be 12.26 mg S g^{-1}. The above results suggested that there was an optimal doping amount of Co species existing in the bimetallic MOF for adsorption desulfurization.

It is well known that there are large amounts of aromatic hydrocarbons and olefins in real gasoline distillate, acting as competitors in the removal of tiny amount of organic sulfur compounds by adsorption. The effect of competitors on TP adsorption was investigated and the results were illustrated in Fig. 6. It can be seen that the breakthrough volume of Cu/Co-BTC-174 in MG2 (cyclohexene was added as competitor with a molar ratio of cyclohexene to TP of 100) dropped sharply to

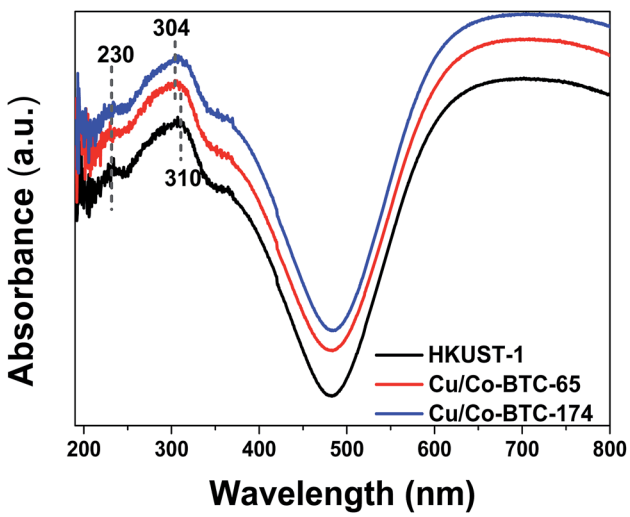

Fig. 4 UV-Vis spectra of HKUST-1 and Cu/Co-BTC samples.

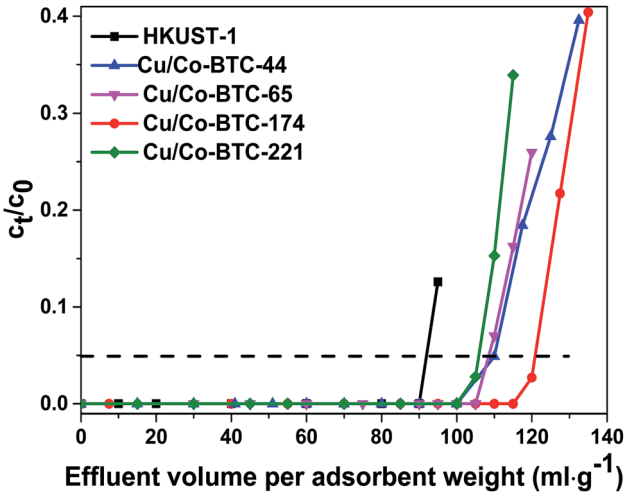

Fig. 5 Adsorption desulfurization of Cu/Co-BTC samples with different Cu/Co ratios.

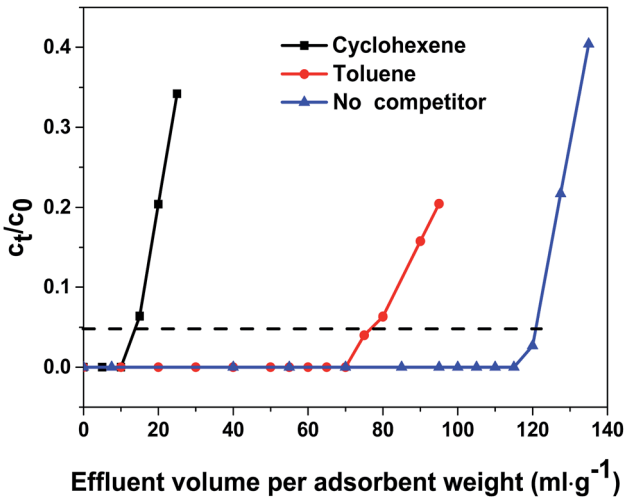

Fig. 6 Effect of toluene and cyclohexene on desulfurization of Cu/Co-BTC-174.

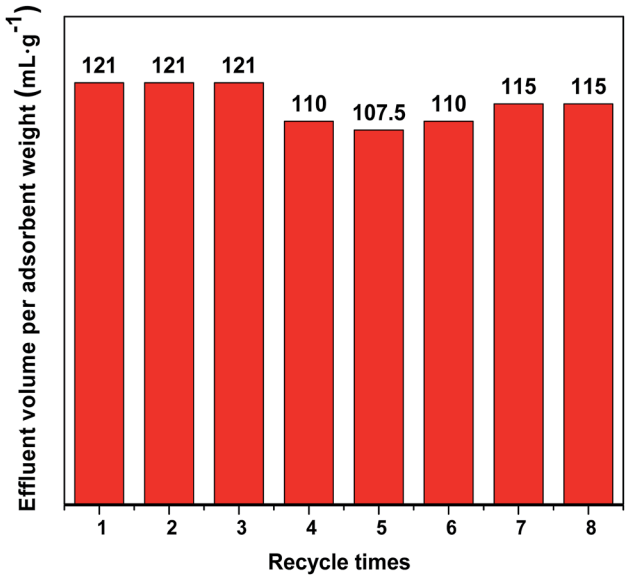

Fig. 7 Reusability of Cu/Co-BTC-174 in fixed-bed adsorption desulfurization.

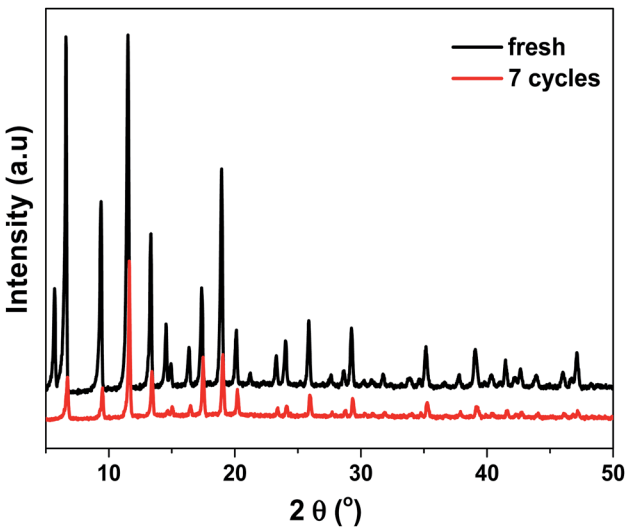

Fig. 8 XRD patterns of fresh Cu/Co-BTC-174 and that recycled for 7 times.

14 mL g^{-1}, while that in MG3 (toluene was added as competitor with a molar ratio of toluene to TP of 100) decreased to 78 mL g^{-1}. The above results showed that Cu/Co-BTC-174 displayed somewhat better desulfurization performance in toluene-rich MG than in cyclohexene-rich one.

3.3 Regeneration of Cu/Co-BTC

The used adsorbent Cu/Co-BTC-174 was subjected to regeneration by purging it in N_2 flow at 423 K for 2 h, and the breakthrough volumes of the fresh and regenerated Cu/Co-BTC-174 were illustrated in Fig. 7. As can be seen, Cu/Co-BTC-174 displayed almost unchanged breakthrough volumes in the first three cycles and only slight decline from 121 to 115 mL g^{-1} in the following several cycles, showing an excellent reusability. After regeneration for seven times, the reused Cu/Co-BTC-174 was characterized by XRD test (Fig. 8). The almost unchanged peak shape and still distinguishable peak intensity of Cu/Co-BTC-174 after seven regenerations indicated that the framework structure was well reserved, leading to an excellent regeneration performance.

4 Conclusions

Doping metal Co in the framework of HKUST-1 has been successfully carried out. This bimetallic organic porous material was characterized by XRD, ICP-AES, UV-Vis, TGA, SEM, and N_2 adsorption. The results showed that only a very small amount of Co ions in the precursors can be successfully introduced into the framework of HKUST-1, and the resultant

bimetallic Cu/Co-BTC showed quite identical properties as HKUST-1 in crystallinity, morphology, pore structure, and heat stability. The newly incorporated Co ions favored TP adsorption because of the synergistic effect, though the mechanism is not clear yet. The adsorbent Cu/Co-BTC-174 exhibited the largest breakthrough sulfur capacity, with an improvement by 30% in comparison to HKUST-1. Cyclohexene addition in model gasoline led to a serious drop in the breakthrough volume of TP adsorption, while toluene resulted in a moderate decline, suggesting that Cu/Co-BTC-174 displayed better desulfurization performance in toluene-rich model gasoline than in cyclohexene-rich one. Cu/Co-BTC displayed excellent regeneration performance, more than 90% of the sulfur uptake capacity was recovered after seven regenerations. The above results enlighten us that synthesizing multi-metal MOFs and taking advantage of the merits of each metal may be a promising approach to improve the adsorption desulfurization performance of MOF-type adsorbents.

Conflicts of interest

There are no conflicts to declare.

Acknowledgements

We are grateful to the financial supports from Natural Science Foundation of China – Liaoning United Funds (grant no. U1508205), Fundamental Research Funds for the Central Universities (grant no. DUT15ZD113), and the Key Laboratory of Applied Surface and Colloid Chemistry (Shanxi Normal University).

References

1 M. Seredych, J. Rawlins and T. J. Bandosz, *Ind. Eng. Chem. Res.*, 2011, **50**, 14097–14104.
2 R. T. Yang, A. J. Hernández-Maldonado and F. H. Yang, *Science*, 2003, **301**, 79–81.
3 C. S. Song, *Catal. Today*, 2003, **86**, 211–263.
4 I. V. Babich and J. A. Moulijn, *Fuel*, 2003, **82**, 607–631.
5 M. Toba, Y. Miki, Y. Kanda, T. Matsui, M. Harada and Y. J. Yoshimura, *Catal. Today*, 2005, **104**, 64–69.
6 J. A. VallaA, A. Lappas, I. A. Vasalos, C. W. Kuehler and N. J. Gudde, *Appl. Catal., A*, 2004, **276**, 75–87.
7 G. Mohebali and A. S. Ball, *Microbiology*, 2008, **154**, 2169–2183.
8 M. Soleimani, A. Bassi and A. Margaritis, *Biotechnol. Adv.*, 2007, **25**, 570–596.
9 L. Kang, H. Y. Liu, H. J. He and C. P. Yang, *Fuel*, 2018, **234**, 1229–1237.
10 W. S. Zhu, P. W. Wu, Y. H. Chao, H. M. Li, F. Zou, S. H. Xun, F. X. Zhu and Z. Zhao, *Ind. Eng. Chem. Res.*, 2013, **52**, 17399–17406.
11 C. P. Huang, B. H. Chen, J. Zhang, Z. C. Liu and Y. X. Li, *Energy Fuels*, 2004, **18**, 1862–1864.
12 H. Y. Lü, W. Z. Ren, H. Y. Wang, Y. Wang, W. Chen and Z. H. Suo, *Appl. Catal., A*, 2013, **453**, 376–382.
13 C. M. Meng, Y. M. Fang, L. J. Jin and H. Q. Hu, *Catal. Today*, 2010, **149**, 138–142.
14 Y. X. Yang, H. Y. Lu, P. L. Ying, Z. X. Jiang and C. Li, *Carbon*, 2007, **45**, 3042–3044.
15 Y. C. Shi, X. J. Yang, F. P. Tian, C. Y. Jia and Y. Y. Chen, *J. Nat. Gas Chem.*, 2012, **21**, 421–425.
16 Y. C. Shi, W. Zhang, H. X. Zhang, F. P. Tian, C. Y. Jia and Y. Y. Chen, *Fuel Process. Technol.*, 2013, **110**, 24–32.
17 F. P. Tian, Q. C. Shen, Z. K. Fu, Y. H. Wu and C. Y. Jia, *Fuel Process. Technol.*, 2014, **128**, 176–182.
18 Y. Yin, D. M. Xue, X. Q. Liu, G. Xu, P. Ye, M. Y. Wu and L. B. Sun, *Chem. Commun.*, 2012, **48**, 9495–9497.
19 W. L. Li, H. Tang, T. Zhang, Q. Li, J. M. Xing and H. Z. Liu, *Am. Inst. Chem. Eng.*, 2010, **56**, 1391–1396.
20 K. A. Cychosz, A. G. Wong-foy and A. J. Matzger, *J. Am. Chem. Soc.*, 2008, **130**, 6938–6939.
21 J. X. Qin, P. Tan, Y. Jiang, X. Q. Liu, Q. X. He and L. B. Sun, *Green Chem.*, 2016, **18**, 3210–3215.
22 H. Sun, X. Han, K. F. Liu, B. X. Shen, J. *C. Liu, D. Wu and X. Y. Shi, *Ind. Eng. Chem. Res.*, 2017, **56**, 9541–9550.
23 N. A. Khan and S. H. Jhung, *J. Hazard. Mater.*, 2012, **237–238**, 180–185.
24 N. A. Khan, Z. Hasan and S. H. Jhung, *Chem.–Eur. J.*, 2014, **20**, 376–380.
25 N. A. Khan, Z. Hasan and S. H. Jhung, *Chem. Commun.*, 2016, **52**, 2561–2564.
26 N. A. Khan, J. W. Jun, J. H. Jeong and S. H. Jhung, *Chem. Commun.*, 2011, **47**, 1306–1308.
27 J. Hu, H. J. Yu, W. Dai, X. Y. Yan, X. Hu and H. Huang, *RSC Adv.*, 2014, **4**, 35124–35130.
28 T. T. Wang, X. X. Li, W. Dai, Y. Y. Fang and H. Huang, *J. Mater. Chem. A*, 2015, **3**, 21044–21050.
29 G. H. Zhao, Q. Liu, N. Tian, L. Yu and W. Dai, *Energy Fuels*, 2018, **32**, 6763–6769.
30 T. T. Wang, Y. Y. Fang, W. Dai, L. F. Hu, N. Ma and L. Yu, *RSC Adv.*, 2016, **6**, 105827–105832.
31 F. P. Tian, Z. K. Fu, H. Zhang, J. J. Zhang, Y. Y. Chen and C. Y. Jia, *Fuel*, 2015, **158**, 200–206.
32 F. P. Tian, Q. F. Ru, C. X. Qiao, X. Sun, C. Y. Jia, Y. Wang and Y. F. Zhang, *J. Energy Chem.*, 2019, **32**, 8–14.
33 D. Peralta, G. Chaplais, A. Simon-Masseron, K. Barthelet and G. D. Pirngruber, *Energy Fuels*, 2012, **26**, 4953–4960.
34 W. J. Tang, J. L. Gu, H. L. Huang, D. H. Liu and C. L. Zhong, *Am. Inst. Chem. Eng.*, 2016, **62**, 4491–4496.
35 H. Sun, X. Han, K. F. Liu, B. X. Shen, J. C. Liu, D. Wu and X. Y. Shi, *Ind. Eng. Chem. Res.*, 2017, **56**, 9541–9550.
36 T. R. C. Van Assche, T. Duerinck, J. J. G. Sevillano, S. Calero, G. V. Baron and J. F. M. Denayer, *J. Phys. Chem. C*, 2013, **117**, 18100–18111.
37 E. Borfecchia, S. Maurelli, D. Gianolio, E. Groppo, M. Chiesa, F. Bonino and C. Lamberti, *J. Phys. Chem. C*, 2012, **116**, 19839–19850.
38 L. Zhang, L. Liu, M. Li, C. Huang, H. Xu, H. W. Hou and Y. T. Fan, *Polyhedron*, 2014, **83**, 197–204.